Particle Accelerators, 1993, Vol. 41, pp 71–91
Reprints available directly from the publisher
Photocopying permitted by license only

EFFECTS OF A TYPE-3 SNAKE AND THE $G\gamma = 2$ IMPERFECTION RESONANCE ON THE SPIN MOTION IN A PROTON SYNCHROTRON

M.G. MINTY* AND S.Y. LEE

Indiana University Cyclotron Facility, Bloomington, Indiana 47405

(Received 27 July 1992)

Experiments with polarized protons performed at the Indiana University Cyclotron Facility (IUCF) Cooler Ring revealed an apparent 1.9 MeV downward shift in the energy at which the $G\gamma = 2$ imperfection resonance occurred. The shift in the resonance energy was resulted from the presence of a type-3 snake due to the electron beam confinement magnets in the cooling region. In the immediate vicinity of the resonance, the interference between the type-3 snake and the $G\gamma = 2$ imperfection resonance was found to be important explaining the asymmetry in the experimental data. The imperfection resonance strength parameters affecting the spin motion were deduced.

1 INTRODUCTION

Spin is a fundamental property of elementary particles. The study of polarized proton collisions contributes to the understanding of the proton substructure and of fundamental interactions between elementary particles. However, depolarizing resonances make it difficult to accelerate polarized protons to high energy in circular accelerators. At certain energies horizontal magnetic fields in the accelerator interact coherently with the proton spin thereby depolarizing the beam. As the machine energy is increased in order to probe more deeply into the inner structure of fundamental particles, the number of depolarizing resonances encountered by the orbiting proton increases. Furthermore, the resonance strength generally increases with increasing beam energy.

Due to the cyclic nature of the proton motion in a circular accelerator, depolarizing resonances occur whenever the proton spin tune, ν_s, equals a resonance tune by satisfying

$$\nu_s = n + mP + q\nu_x + r\nu_y + s\nu_{syn}, \tag{1}$$

where P is the superperiodicity (the number of identical ring lattice sections) of the accelerator, which is equal to 1 for the IUCF Cooler Ring, ν_x and ν_y are the horizontal and vertical betatron tunes, ν_{syn} is the synchrotron tune, while m, n, q, r,and s are integers. In the absence of any longitudinal and radial error fields, the spin tune, ν_s, is equal to $G\gamma$, where $G = 1.7928$ is the anomalous part of the proton magnetic moment and γ is the relativistic Lorentz factor.

* Present address: Stanford Linear Accelerator Center, Mailstop 26, P.O. Box 4349, Stanford, CA 94309

The general resonance condition of Eq. (1) can be subdivided into different catagories. Imperfection depolarizing resonances, for which $\nu_s = n$ = integer, arise from magnetic error fields experienced by the orbiting particle. Gradient error and intrinsic resonances, which result from vertical betatron motion in the horizontal fields of quadrupoles, occur if $\nu_s = n + r\nu_y$ and $\nu_s = mP + r\nu_y$, respectively. Synchrotron depolarizing resonances due to the coupling between transverse and longitudinal oscillations occur if $\nu_s = n + s\nu_{syn}$ or $\nu_s = mP + s\nu_{syn}$. Finally, betatron coupling resonances, given by $\nu_s = n + q\nu_x + r\nu_y$ can also result in spin depolarization.

These resonances may be overcome using an arrangement of magnets, called a Siberian snake[1]. A Siberian snake rotates the spin of each proton by 180 degrees about an axis in the horizontal plane on each turn around the ring without changing the closed orbit outside the snake. This forces the spin tune, ν_s, to be $\frac{1}{2}$. The resonance condition of Eq. (1) is therefore never satisfied regardless of the beam energy provided that the betatron tunes avoid half integer orbital resonances.

In order to test the Siberian snake concept, a solenoidal snake was installed in the IUCF Cooler Ring. These tests have shown that the snake is effective in preserving the spin in the presence of imperfection, intrinsic, and synchrotron depolarizing resonances.[2–5] However these experiments revealed a discrepancy between the calibrated Cooler Ring energy and the energy at which the imperfection resonance occurred. By comparison of the experimental data with model calculations, the data revealed a systematic downward shift in the resonance energy of about 1.9 MeV. Since the energy calibration of the Cooler Ring is accurate[6] to better than 10^{-3}, there seemed to be a discrepancy. Recently, the source of this discrepancy was explained by Pollock[7] and Minty *et al.*[8]. The magnetic fields in the electron cooling region of the Cooler Ring constitute[7] a type-3 snake[9], which shifted the proton spin tune. A "type-3 snake", terminology used by Pollock[7], precesses the proton spin about the normal to the ring plane without changing the closed orbit outside the "snake". Thus a type-3 snake is not a snake as conventionally defined.

In this paper, theoretical calculations including effects due to the type-3 snake and the $G\gamma = 2$ imperfection resonance on the spin motion will be compared with experimental data of Ref. 5 and 8. In section 2, we review basic properties of spin motion in a proton synchrotron. In section 3, we use the Thomas-BMT equation to find the closed orbit of the spin vector in the presence of the type-3 snake in the electron cooling region. We will study the parameters affecting the spin tune shift and the corresponding resonance energy shift. In section 4, the existing experimental data will be compared with the analysis of section 3. In section 5, the effect of the $G\gamma = 2$ imperfection resonance on the spin motion of the proton will be studied. In section 6 the combined effects of the type-3 snake and the $G\gamma = 2$ imperfection resonance will be included in data analysis in the immediate vicinity of the resonance. A conclusion will be given in section 7.

2 SPIN MOTION IN A PROTON SYNCHROTRON

The dynamics of spin motion has been treated by many authors[10–17]. In 1927 Thomas[10] showed that a purely kinematic precession governs the behavior of relativistic accelerated particles which possess a magnetic moment. In 1959, Bargmann, Michel, and Telegdi[11]

expressed the magnetic field in terms of its transverse and longitudinal components. The resultant Thomas-BMT equation describes the spin motion in the presence of electromagnetic fields experienced by an orbiting particle in the laboratory frame. For many practical applications, there are no significant electric fields in the accelerator and the Thomas-BMT equation becomes,

$$\frac{d\vec{S}}{dt} = \frac{e}{\gamma m}\vec{S} \times [(1+G\gamma)\vec{B}_{\perp} + (1+G)\vec{B}_{\parallel}], \tag{2}$$

where $\vec{S}$ is the spin vector, e is the electric charge, γ is a relativistic factor, $G = 1.7928$ is the anomalous part of the proton magnetic moment, and $\vec{B}_{\perp}$ and $\vec{B}_{\parallel}$ are respectively the magnetic field components transverse to and parallel to the instantaneous velocity of the particle. Notice that the amount of spin kick due to a transverse magnetic field depends on the particle energy through the factor $1 + G\gamma$. The Thomas-BMT equation can then be transformed to the Frenet-Serret curvilinear coordinate system as[16],

$$\frac{dS_x}{d\theta} = -\kappa S_s - rS_y; \quad \frac{dS_s}{d\theta} = +\kappa S_x - tS_y; \quad \frac{dS_y}{d\theta} = +rS_x + tS_s, \tag{3}$$

Here S_x, S_s and S_z are components of spin vectors in the curvilinear coordinate system in which $\hat{x}$ is radially outward, $\hat{s}$ is along the beam direction, $\hat{y}$ is vertical, and ρ is the local radius of curvature of the reference orbit. The angle θ is the turning angle of the reference orbit, and κ, r, and t are functions of the transverse coordinates of the particle orbit given by[16] $\kappa = G\gamma - (1+G\gamma)\rho x'' \approx G\gamma$; $r = (1+G\gamma)y' - \rho(1+G)(\frac{y}{\rho})'$; $t = (1+G\gamma)\rho y''$, where the primes denote derivatives with respect to the longitudinal coordinate, s. Eq. (3) can be transformed into an equivalent spinor representation with

$$\frac{d\Psi}{d\theta} = -\frac{i}{2}\begin{pmatrix} \kappa & t+ir \\ t-ir & -\kappa \end{pmatrix}\Psi. \tag{4}$$

Here Ψ is a two-component complex spinor. The polarization components may be obtained by taking the expectation value of the Pauli matrix vector, $\vec{\sigma}$; i.e.

$$S_i = \Psi^{\dagger}\sigma_i\Psi, \tag{5}$$

3 SPIN MOTION IN THE PRESENCE OF THE TYPE-3 SNAKE IN THE COOLER

Fig. 1 shows spin precession elements in the cooling section of the Cooler Ring. The orbiting proton experiences the following progression of precessing fields in the cooling region: VS-CS-VS′-T-MS-T-VS′-CS-VS. Here MS is the main cooling solenoid, T are toroids which match the electron beam injection and extraction trajectory to that of the proton in MS, CS are compensating solenoids which are set to cancel the coupling of the betatron motion introduced by the main solenoid, and VS and VS′ are vertical steerers which remove vertical orbit perturbations introduced by the radial part of the toroidal field. The fields due to the weaker horizontal steerers have a negligible effect on the

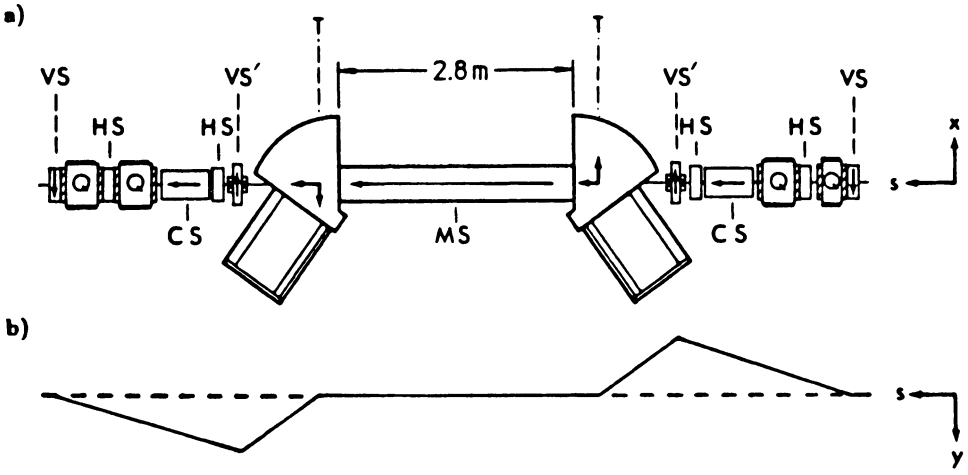

FIGURE 1: Cooling Region Transport Elements. a) Top view: Orbiting protons travel collinearly with the cooling electrons in the main solenoid (MS). The electron beam is directed into and out of the path of the protons by two toroids (T). The two compensating solenoids (CS) are designed to cancel the coupling of the betatron motion introduced by the main solenoid. The vertical steerers (VS) and (VS)′ remove vertical orbit perturbations introduced by the radial part of the toroidal field. The fields due to the weaker horizontal steerers (HS) are found to be negligible in their effect on the spin motion of the proton. b) Side view: The orbit deflections experienced by the protons due to the magnets in the cooling region are shown.

spin motion of the proton. In the following calculations, in order to maintain a collinear alignment of the proton and electron beams in the main cooling solenoid, it is assumed that the spin precession introduced by VS is exactly cancelled by the spin precession due to the radial fields in VS′ and T. Neglecting the contribution from the imperfection resonance, the spin equation of motion for a single turn around the accelerator in the presence of the electron cooling system becomes,

$$e^{-i\pi\nu_s(\vec{n}_s\cdot\vec{\sigma})} = e^{-i\frac{G\gamma}{2}(2\pi-\theta)\sigma_y}\ C\ e^{-i\frac{G\gamma}{2}\theta\sigma_y}, \tag{6}$$

where ν_s is the spin tune, $\vec{n}_s \equiv (\cos\alpha_x, \cos\alpha_s, \cos\alpha_y)$ is the stable spin direction vector, θ is now the angle at which the polarization detectors are located relative to the cooling section ($\theta = \pi/3$), and C is the matrix defining the spin precession in the cooling region, given by

$$C = [e^{-i\frac{\phi}{2}\sigma_x} e^{i\frac{\psi_c}{4}\sigma_s} e^{i\frac{\phi}{2}\sigma_x}] e^{-i\frac{\psi}{2}\sigma_s} [e^{-i\frac{\phi}{2}\sigma_x} e^{i\frac{\psi_c}{4}\sigma_s} e^{i\frac{\phi}{2}\sigma_x}], \tag{7}$$

Here ψ, ψ_c, and ϕ are the precession angles due to the cooling solenoid, the compensating solenoids, and the vertical steerers, respectively.

The effective solenoidal precession angle, $\psi_c - \psi$, in the cooling region is given by

$$\psi_c - \psi = \frac{(1+G)}{B\rho}[(1.3072 I_{comp}) - (0.3279 I_{tor} + 0.4065 I_{main})] \tag{8}$$

in which I_{comp} [kA] is the current in the compensating solenoids which are wired in series, I_{tor} [kA] is the current in the toroids which are also wired in series, and I_{main}

[kA] is the current in the main cooling solenoid. The factor $B\rho$ is the magnetic rigidity [T-m].

By expanding the expressions on both sides of Eq. (6), the components of the stable spin direction are given by

$$\begin{aligned}
\cos\alpha_y &= \frac{1}{\sin\pi\nu_s}[(\cos\frac{\psi}{2}\cos\frac{\psi_c}{2}+\sin\frac{\psi}{2}\sin\frac{\psi_c}{2}\cos\phi)\sin\pi G\gamma \\
&\quad \frac{1}{\sin\pi\nu_s}[\cos\frac{\psi}{2} -(\cos\frac{\psi}{2}\sin\frac{\psi_c}{2}\sin\phi+\sin\frac{\psi}{2}\sin^2\frac{\psi_c}{4}\sin 2\phi)\cos\pi G\gamma], \\
\cos\alpha_s &= \frac{1}{\sin\pi\nu_s}[-\cos\frac{\psi}{2}\sin\frac{\psi_c}{2}\cos\phi+(\cos^2\frac{\psi_c}{4}-\sin^2\frac{\psi_c}{4}\cos 2\phi)\sin\frac{\psi}{2}]\cos\frac{2G\gamma\pi}{3} \\
\cos\alpha_x &= \frac{1}{\sin\pi\nu_s}[\cos\frac{\psi}{2}\sin\frac{\psi_c}{2}\cos\phi-(\cos^2\frac{\psi_c}{4}-\sin^2\frac{\psi_c}{4}\cos 2\phi)\sin\frac{\psi}{2}]\sin\frac{2G\gamma\pi}{3}.
\end{aligned} \tag{9}$$

The spin tune, ν_s given by the trace of Eq. (6),

$$\begin{aligned}
\cos\pi\nu_s &= [\cos\frac{\psi_c}{2}\cos\frac{\psi}{2}+\sin\frac{\psi_c}{2}\sin\frac{\psi}{2}\cos\phi]\cos(\pi G\gamma) \\
&\quad +[\cos\frac{\psi}{2}\sin\frac{\psi_c}{2}\sin\phi+\sin\frac{\psi}{2}\sin^2\frac{\psi_c}{4}\sin 2\phi]\sin(\pi G\gamma),
\end{aligned} \tag{10}$$

depends on the three spin precession angles ψ, ψ_c, and ϕ in the cooling region and on the incident beam energy. At fixed energy, the spin tune may depend sensitively on the effective steerer precession angle, ϕ. The dependence of the spin tune on this angle is shown in Fig. 2 as a function of beam energy when the longitudinal parameters are fully compensated and a typical values of ψ equal to 0.7503 rad for the solenoid is assumed.

When the transverse steerers are turned off, $\phi = 0$, the spin tune reduces to[2]

$$\cos\pi\nu_s = \cos\frac{\psi_c-\psi}{2}\cos\pi G\gamma.$$

The additional terms in Eq. (10) introduce a shift in the spin tune and is a result of the noncommutativity of the spin precession between the steerers and the longitudinal cooling solenoid.

Assuming that the injected polarization is purely vertical, the observed polarization is determined by first projecting the injected polarization onto the stable spin direction and then projecting the projected polarization onto the polarimeter. The effects due to a slightly misaligned injected polarization are analyzed in appendix A and are shown to be negligible in the vicinity of $\psi - \psi_c \approx 0$. The radial, longitudinal, and vertical components of the polarization are then

$$P_R = P_{inj}\cos\alpha_y\cos\alpha_x, \quad P_L = P_{inj}\cos\alpha_y\cos\alpha_s, \quad P_V = P_{inj}\cos^2\alpha_y, \tag{11}$$

where only P_R and P_V components of the polarization vector can be measured. They are given by

$$\begin{aligned}
P_R &= P_{inj}\frac{\sin\frac{2G\gamma\pi}{3}\cos\alpha_y}{\sin\pi\nu_s}\{\cos\frac{\psi}{2}\sin\frac{\psi_c}{2}\cos\phi-(\cos^2\frac{\psi_c}{4}-\sin^2\frac{\psi_c}{4}\cos 2\phi)\sin\frac{\psi}{2}\} \\
P_V &= P_{inj}\cos^2\alpha_y,
\end{aligned} \tag{12}$$

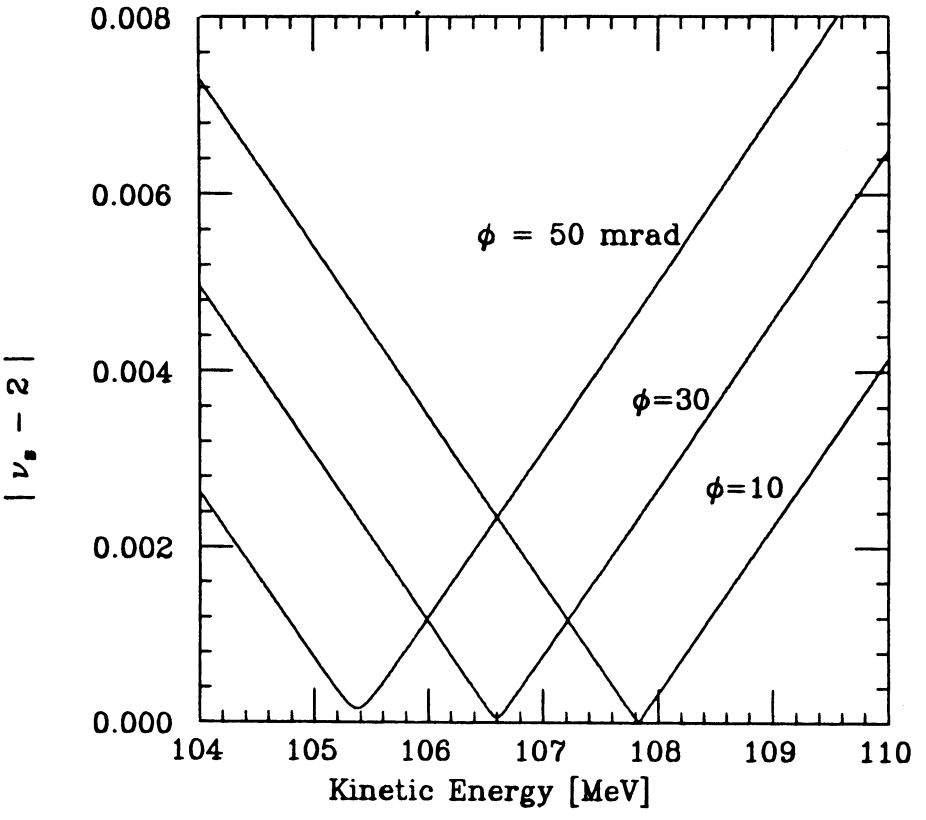

FIGURE 2: Spin Tune vs. Beam Energy with a Type-3 Snake. Eq. (10) is used to show the dependence of the spin tune, ν_s, on steerer precession angle, ϕ, with beam energies near the resonance energy. The longitudinal imperfection field is assumed to be fully compensated. The dotted curve corresponds to $\phi = -10$ mrad, the solid curve to $\phi = -30$ mrad, and the dashes curve to $\phi = -50$ mrad. With a -30 mrad effective precession angle, the spin tune is observed to be shifted from 2.0000 by about 0.0036 at 108.4 MeV. The corresponding resonance energy is near 106.5 MeV.

with

$$\cos\alpha_y = \{[\cos\tfrac{\psi}{2}\cos\tfrac{\psi_c}{2} + \sin\tfrac{\psi}{2}\sin\tfrac{\psi_c}{2}\cos\phi]\sin\pi G\gamma - [\cos\frac{\psi}{2}\sin\frac{\psi_c}{2}\sin\phi + \sin\frac{\psi}{2}\sin^2\frac{\psi_c}{4}\sin 2\phi]\cos\pi G\gamma\}\frac{}{\text{si}}$$

The magnitudes of the spin precession angles, ϕ, ψ, and ψ_c in the vertical steerers, the cooler solenoid, and the compensating solenoids, respectively, are relatively small. Using the small angle approximation for ϕ, Eqs. (10,12,13) reduce to

$$\cos\pi\nu_s \approx \cos\frac{\psi_c - \psi}{2}\cos(\pi G\gamma - \frac{\psi\phi}{2}) \tag{14}$$

$$P_R \approx P_{inj}\sin\frac{\psi_c - \psi}{2}\sin(\frac{2G\gamma\pi}{3})\frac{\cos\alpha_y}{\sin\pi\nu_s}; \quad P_v \approx P_{inj}\cos^2\alpha_y, \tag{15}$$

$$\cos\alpha_y \approx \cos(\frac{\psi_c - \psi}{2})\sin(\pi G\gamma - \frac{\psi\phi}{2})\frac{1}{\sin\pi\nu_s} \tag{16}$$

Eq. (14) indicates that the spin tune is shifted from the expected value of $G\gamma$ to $G\gamma - \frac{\psi_c\phi}{2\pi}$. Therefore the imperfection depolarizing resonance will occur when $G\gamma - \frac{\psi_c\phi}{2\pi} = n$ with integer n. The shift in the spin tune leads to a shift in the resonance energy, ΔE, which is given by

$$\Delta E = mc^2\Delta\gamma = mc^2\frac{\psi_c\phi}{2\pi G}. \tag{17}$$

The approximations of Eqs. (14-16) for the components of the polarization show that the spin motion may be described by a simple spin tune shift resulting from the type-3 snake. Notice however that in making the small precession angle approximation, a small higher order asymmetry is neglected; the approximations predict a symmetry in the vertical and radial polarizations about the fully compensated longitudinal field value, whereas the explicit formulas for the polarization components do not. In summary, noncommutativity of the spin precession matrices between the steerers and the longitudinal compensating solenoids gives rise to a shift in the spin tune. Because the spin tune is changed without affecting the spin closed orbit outside the snake, to lowest order, this arrangement of magnets was called a type-3 snake.

From Eq.(14), the ratio of the radial polarization to the vertical polarization can be expressed as

$$\frac{P_R}{P_V} = \frac{\sin\frac{2G\gamma\pi}{3}}{\sin\pi[G\gamma - \frac{\phi\psi}{2\pi}]} \times \sin\frac{\psi_c - \psi}{2} \approx \frac{\sin\frac{2G\gamma\pi}{3}}{2\sin\pi[G\gamma - \frac{\phi\psi}{2\pi}]}(\psi_c - \psi),$$

which is linear with respect to the solenoidal field error $\psi_c - \psi$. The slope of P_R/P_V vs $(\psi_c - \psi)$ is inversely proportional to the deviation of the spin tune from an integer. This method was used to determine the spin tune shift due to the type 3 snake in Ref. 8.

4 COMPARISON TO EXPERIMENTAL DATA

Vertically polarized proton beams with energies ranging from about 104 to 120 MeV were injected, stored, cooled, stacked, and spin analyzed at the Indiana University Cyclotron Facility (IUCF) Cooler Ring. The results of the analysis along with experimental data[5,8] are presented in Fig. 3. Shown are the data taken at 104.5, 105.9, 106.9, 107.8, and 110.5 MeV. Plotted on the left are the measured values of the vertical polarization, and on the right, the radial polarization. The sharp dips in the polarization data at 104.5 and 107.8 MeV correspond to synchrotron depolarization resonances[3] and are not included in the present analysis.

The solid curves are calculated using Eqs. (12,13), which include the effects of the type-3 snake in the electron cooling region assuming zero closed orbit error elsewhere in the ring. The dotted curves indicate the predicted behavior taking into account only the longitudinal field imperfection in Eqs. (12,13) with zero vertical steerer angle ϕ (i.e. with the type-3 snake off). The resonance energy lies between 105.9 and 106.9 MeV as can be seen by the change in the sign of the radial polarization. The offset in the

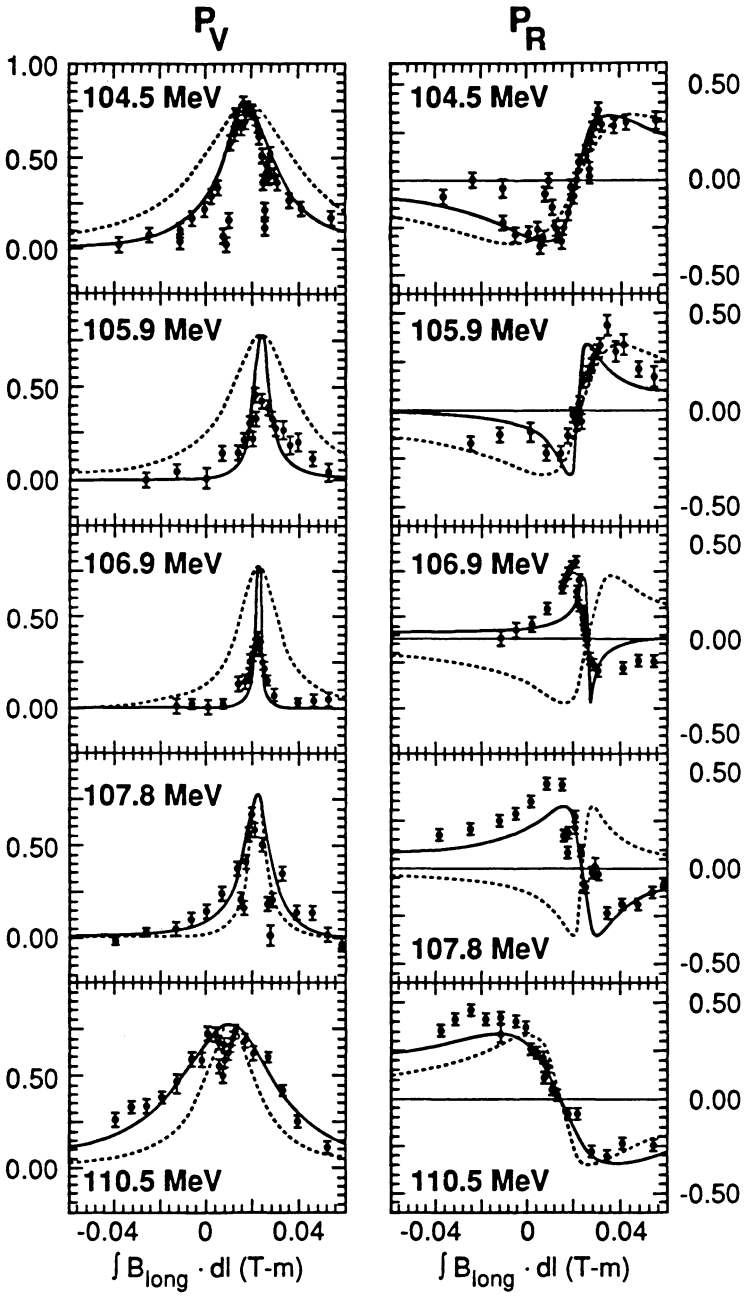

FIGURE 3: Type-3 Snake Data[5,8] and Model Calculations for 5 Different Measurements at Fixed Energies Near the $G\gamma = 2$ Imperfection Resonance with Vertically Polarized Injected Beam. The measured vertical and radial polarization are plotted as a function of the longitudinal field error. The solid curves are obtained from Eqs. (12-13) and include the effect of the type-3 snake in the cooling region. The dashed curves are obtained with the type-3 snake turned off; i.e. $\phi = 0$.

longitudinal field error was not taken into account and the curves were translated along the horizontal axis to allow for comparison.

The precession angles in the main and compensating solenoids are obtained from Eq. (8) using the known operating currents. The precession angle in the steerers was determined, using a global fit to the data, to be -30 mrad at all incident beam energies except for the data taken during the earlier stages of cooler development. The fitted steerer angle at 104.2 MeV was -53 mrad and -39 mrad at 104.6 MeV. The value of the precession angle depends on the operating parameters of the accelerator at the time the data were taken.

The shift in the spin tune due to the type-3 snake is approximately $-\frac{\psi\phi}{2\pi}$. With $\phi = -30$ mrad and an average value of $\psi = 0.7503$ rad, the spin tune was shifted by about 0.0036. The shift in the spin tune corresponds to a shift in the resonance energy of -1.9 ± 0.2 MeV, where ± 0.2 MeV reflects variations about this observed offset, the variations in ϕ obtained from the global fit, and the variations in ψ.

Upon close inspection of the region near the imperfection resonance, it is clear that the experimental data in the 105 to 108 MeV energy range can not be explained by the above calculations. The discrepancy may arise from the effects of the nearby imperfection resonance. In the following section we study the effect of the imperfection resonance on the spin motion of the proton.

5 EFFECT OF THE $G\gamma = 2$ IMPERFECTION RESONANCE

Along with the type-3 snake, the transverse imperfection resonance may also shift the spin tune. In the single resonance approximation, i.e. $t + ir = \epsilon e^{-iK\theta}$, Eq.(4) can be transformed[18] to the resonance precession frame with

$$\Psi_k = e^{i\frac{K\theta}{2}\sigma_y}\Psi. \tag{18}$$

We obtain

$$\frac{d\Psi_k}{d\theta} = \frac{i}{2}(\delta\sigma_y + \epsilon_R\sigma_x - \epsilon_I\sigma_s)\Psi_k, \tag{19}$$

where $\delta = K - G\gamma$ and $\epsilon = \epsilon_R + i\epsilon_I$ is the resonance strength. Eq. (19) can be integrated easily to obtain

$$\Psi_k(\theta_f) = e^{\frac{i}{2}(\delta\sigma_y+\epsilon_R\sigma_x-\epsilon_I\sigma_s)(\theta_f-\theta_i)}\Psi_k(\theta_i). \tag{20}$$

Transforming back to the particle rest frame, we obtain then

$$\Psi(\theta_f) = e^{-i\frac{K\theta_f}{2}\sigma_y}e^{\frac{i}{2}(\delta\sigma_y+\epsilon_R\sigma_x-\epsilon_I\sigma_s)(\theta_f-\theta_i)}e^{i\frac{K\theta_i}{2}\sigma_y}\Psi(\theta_i) = T(\theta_f,\theta_i)\Psi(\theta_i). \tag{21}$$

By expanding the exponential, the spin transfer matrix $T(\theta_f, \theta_i)$ for a single resonance may be calculated[18]:

$$T(\theta_f,\theta_i) = \begin{pmatrix} ae^{i(c-\frac{K(\theta_f-\theta_i)}{2})} & ibe^{-i(d+\frac{K(\theta_f+\theta_i)}{2})} \\ ibe^{i(d+\frac{K(\theta_f+\theta_i)}{2})} & ae^{-i(c-\frac{K(\theta_f-\theta_i)}{2})} \end{pmatrix} \tag{22}$$

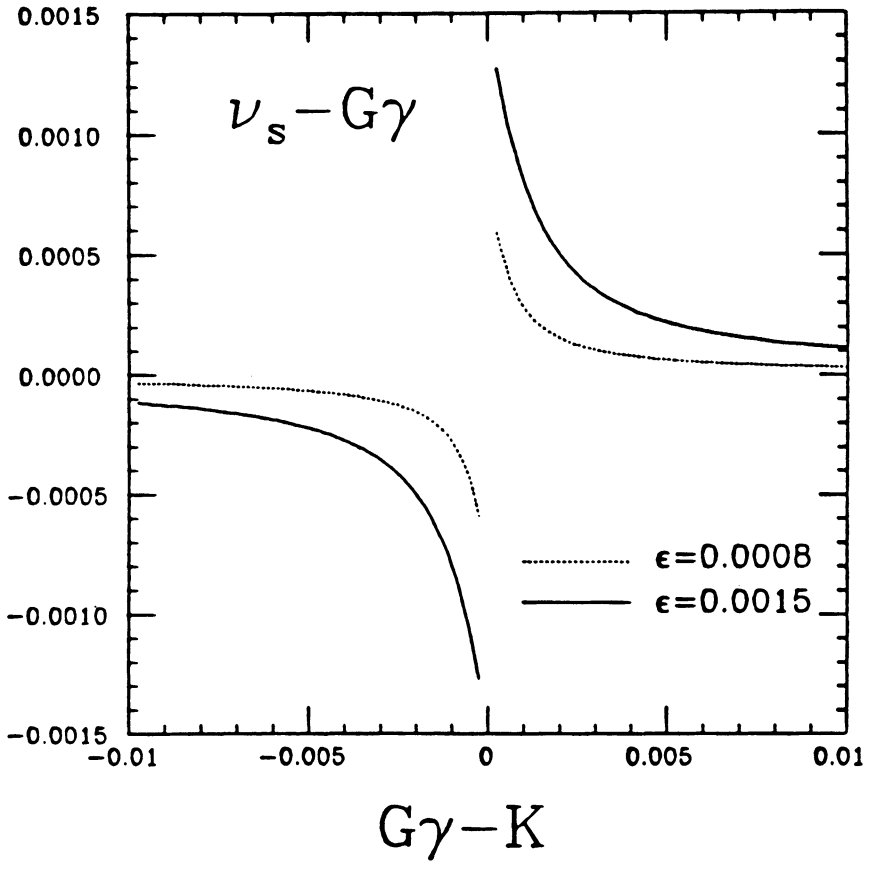

FIGURE 4: Spin Tune Shift vs. $G\gamma - 2$ Near an Imperfection Resonance. From Eq. (24) the dependence of the shift in the spin tune on $G\gamma - 2$ due to an imperfection resonance is plotted. The dashed curve corresponds to a resonance strength of magnitude 0.0008. The solid curve results for a resonance strength of 0.0015.

with

$$b = \frac{|\epsilon|}{\lambda} \sin \frac{\lambda(\theta_f - \theta_i)}{2}, \quad a = \sqrt{1 - b^2}, \quad c = \arctan[\frac{\delta}{\lambda} \tan \frac{\lambda(\theta_f - \theta_i)}{2}], \quad (23)$$
$$d = \arg\epsilon^*, \quad \delta = K - G\gamma, \quad \lambda = \sqrt{\delta^2 + |\epsilon|^2}.$$

The spin tune can be obtained from the trace of the one turn transfer map, $T(\theta + 2\pi, \theta)$ of Eq. (22), i.e.

$$\cos \pi\nu_s = a \cos(c - K\pi). \quad (24)$$

Figure 4 shows the effect of the spin tune shift, $K - G\gamma$, as a function of $G\gamma - 2$ for the special cases where $|\epsilon| = \sqrt{\epsilon_R^2 + \epsilon_I^2} = 0.0008$ and $|\epsilon| = 0.0015$. In both cases, for $G\gamma$ far away from the resonance tune, K, i.e. $\delta >> |\epsilon|$ and $a \approx 1$, we obtain $\nu_s \approx G\gamma$. As $G\gamma$

approaches the resonance tune, the spin tune is shifted from $G\gamma$ by $\Delta\nu_s = -|\epsilon|$ below the resonance and by $\Delta\nu_s = |\epsilon|$ above the resonance; i.e. the spin tune is always shifted *away* from the resonance tune. Therefore at a given energy, the observed width of the vertical polarization (see Fig. 3) would always be increased due to the presence of the imperfection resonance. The observed slope of the radial polarization through the fully compensated field value would also be lessened in magnitude. Figure 4 also shows that the effect of the imperfection resonance becomes important only in very close proximity to the resonance.

6 EFFECT OF THE TYPE-3 SNAKE AND THE $G\gamma = 2$ IMPERFECTION RESONANCE

The periodic solution to the spin equation of motion in the presence of both the type-3 snake in the electron cooling system and the $G\gamma = 2$ imperfection resonance may be expressed using the spin precession matrix of the cooling section, C, defined in Eq. (7) and the transfer matrix, T, defined in Eq. (22). The solution may be calculated by expanding

$$e^{-i\pi\nu_s(\vec{n}_s\cdot\vec{\sigma})} = T(\theta_0 + 2\pi, \theta_0 + \frac{\pi}{3})\ C\ T(\theta_0 + \frac{\pi}{3}, \theta_0). \tag{25}$$

After some algebra, the components of the resultant polarization vector may be obtained:

$$\begin{aligned}\cos\pi\nu_s &= [a_1a_2\cos\pi G\gamma - b_1b_2]{C_R}^{1,1} + [a_1a_2\sin\pi G\gamma]{C_I}^{1,1} \\ &\quad + [a_2b_1\sin(\frac{5\pi G\gamma}{6} - \chi) - a_1b_2\sin(\frac{\pi G\gamma}{6} + \chi)]{C_R}^{1,2},\end{aligned} \tag{26}$$

$$\begin{aligned}P_R &= P_{inj}\{-[a_2b_1\cos(\frac{5\pi G\gamma}{6} + \chi) + a_1b_2\cos(\frac{\pi G\gamma}{6} - \chi)]{C_R}^{1,1} \\ &\quad - [a_2b_1\sin(\frac{5\pi G\gamma}{6} + \chi) + a_1b_2\sin(\frac{\pi G\gamma}{6} - \chi)]{C_I}^{1,1} \\ &\quad + [a_1a_2\sin\frac{2\pi G\gamma}{3} + b_1b_2\sin 2\chi]{C_R}^{1,2}\}\frac{\cos\alpha_y}{\sin\pi\nu_s},\end{aligned} \tag{27}$$

$$P_V = P_{inj}\cos^2\alpha_y, \tag{28}$$

where the ${C_R}^{i,j}$ and ${C_I}^{i,j}$ are the real and imaginary parts of the (i,j)-th element of the transfer matrix, C, given in Eq. (7). Here $\chi = d + 2\theta_0 + \frac{\pi}{3}$, and

$$\begin{aligned}\cos\alpha_y &= \{[a_1a_2\sin\pi G\gamma]{C_R}^{1,1} - [a_1a_2\cos\pi G\gamma + b_1b_2]{C_I}^{1,1} \\ &\quad + [a_1b_2\cos(\frac{\pi G\gamma}{6} + \chi) - a_2b_1\cos(\frac{5\pi G\gamma}{6} - \chi)]{C_R}^{1,2}\}\frac{1}{\sin\pi\nu_s}\end{aligned} \tag{29}$$

with

$$b_1 = \sqrt{1 - a_1^2} = \frac{|\epsilon|}{\lambda}\sin\frac{\pi\lambda}{6} \approx \frac{\pi|\epsilon|}{6}; \quad b_2 = \sqrt{1 - a_2^2} = \frac{|\epsilon|}{\lambda}\sin\frac{5\pi\lambda}{6} \approx \frac{5\pi|\epsilon|}{6}. \tag{30}$$

The effects of the $G\gamma = 2$ imperfection depolarizing resonance may be understood qualitatively by comparison of Eqs. (26-28), which include resonance effects, to Eqs.

(10,12,13), in which only the type-3 snake is considered. Note that the resonance strength, $|\epsilon|$, and phase, d =argϵ^*, depend critically on the vertical closed orbit of the beam. Experiments performed during different running periods may not be expected to have the same resonance strength. Earlier imperfection resonance studies carried out at the AGS[19] illustrate this point. We expect the resonance parameters to be different at the different energies (except for the 106.9 and 107.8 MeV data which were taken during the same running period) because special care in maintaining similar closed orbits for the different running periods was not exercised and because ring lattice properties may have changed between running periods.

To understand effects of the imperfection resonance on the polarization, we will make a small angle approximation for ϕ, the vertical steerer in the cooling region, and linear approximation in $|\epsilon|$ for b_1, b_2 of Eq.(30). The radial polarization becomes,

$$P_R \approx -P_{inj}[\sin\frac{\psi-\psi_c}{2}\sin\frac{2\pi G\gamma}{3}+|\epsilon|\pi\cos\frac{\psi-\psi_c}{2}\cos(d+2\theta_0)]\frac{\cos\alpha_y}{\sin\pi\nu_s}. \quad (31)$$

Note here that the radial polarization exhibits an asymmetry in $\psi-\psi_c$ of the longitudinal field error of Eq.(8). The asymmetry will be more pronounced for $d+2\theta_0 = n\pi$ with integer n. From Eq. (31) one might argue that the asymmetry would be more important for a larger resonance strength. However, at a larger resonance strength, the spin closed orbit is tilted away from the vertical axis. Because the injected polarization is vertical, the initial polarization will become smaller due to a smaller initial projection. The total radial polarization would therefore be reduced and the asymmetry would be less pronounced. Similarly, the vertical polarization is given by,

$$P_v \approx \frac{P_{inj}}{\sin^2\pi\nu_s}\{\cos\frac{\psi-\psi_c}{2}\sin(\pi G\gamma-\frac{\psi_c\phi}{2})+\frac{2\pi|\epsilon|}{3}\sin\frac{\psi_c-\psi}{2}\cos(d+2\theta_0+\frac{2\pi}{3})\}^2, \quad (32)$$

which also exhibits asymmetry as a function of $\psi-\psi_c$ of the longitudinal field error.

The asymmetry in both the radial and vertical polarization, arising from the interference between the longitudinal imperfection field error and the transverse field errors, is linear in $\psi_c-\psi$. On the other hand, asymmetry may also result from the polarization vector mismatch at injection. Appendix A shows that the asymmetry of the radial polarization, due to the polarization vector mismatch at the injection, is of second order in the $\psi-\psi_c$ field error. From the experimental data, we observe that the asymmetry in the radial polarization is much more pronounced than that of the vertical polarization. Thus the asymmetry for small $\psi_c-\psi$ may not due to a mismatch at injection.

Since the spin tune is shifted away from the resonance by an amount $|\epsilon|$ near the resonance position (see section 5), the denominator containing $\sin\pi\nu_s$ will be correspondingly larger. The peak vertical polarization of Eq. (32) will therefore be reduced with an increase in the resonance strength.

The resonance strength, $|\epsilon|$, and the phase angle, $d+2\theta_0$, may be uniquely determined by fitting the polarization data. Here θ_0 represents the relative orbital angle in the ring. In our case, we take θ_0 to be zero and represent the combined effects of the resonance phase and orbital phase by d. Hence $|\epsilon|$ and argϵ^* seem sufficient in characterizing the effects on the spin motion due to the imperfection resonance.

The imperfection resonance strength at the IUCF Cooler Ring is expected[20] to be on the order of 10^{-3}. Thus the effects of the imperfection resonance should be important only in the immediate vicinity of the $G\gamma = 2$ resonance; i.e. at energies ranging from 105 to 108 MeV. Experimental data exists at 105.9, 106.9, and 107.8 MeV.

In the following we analyze experimental data taken in the immediate vicinity of the imperfection resonance. One word of caution is that data taken on different dates may have different imperfection resonance strengths, ϵ_R and ϵ_I, and different orbit steerer angle, ϕ. Both $|\epsilon|$ and $\arg\epsilon^*$ depend upon the operating conditions of the storage ring as they are determined by the perturbing fields that constitute the imperfection resonance. The orbit steerer angle depends on how the electron cooling system was set up at the time in which the data were taken.

6.1 Data Analysis for 105.9 MeV Incident Beam Energy

Using the three parameters that govern the spin motion (ϕ, the precession angle in the steerers in the cooling region, $|\epsilon|$, the magnitude of the imperfection depolarizing resonance, and $\arg\epsilon^*$, the conjugate of the resonance phase), in Eqs. (26-28), one can fit the data at 105.9 MeV. Fig. 5 shows the experimental data along with model calculations with no type-3 snake (dashed curve), the type-3 snake only (dotted curve), and the type-3 snake along with the $G\gamma = 2$ imperfection resonance (solid curve).

With the type-3 snake turned off ($\phi = 0$), the width of the vertical polarization peak (measured full width at half maximum) is predicted to be too wide and full beam polarization is predicted to be maintained for a fully compensated longitudinal field. With the type-3 snake turned on ($\phi = -25$ mrad) in the absence of the $G\gamma = 2$ imperfection resonance, the polarization profile is predicted to be slightly too narrow and again peaks at full polarization given a fully compensated field. With the type-3 snake turned on ($\phi = -25$ mrad) in the presence of the nearby $G\gamma = 2$ imperfection resonance ($|\epsilon| = 0.0015, \arg\epsilon^* = 4.5$ rad), both the vertical and the radial polarizations are fairly fit by the model calculation. The asymmetry in the radial polarization and the reduction in the magnitude of the vertical polarization can be reproduced. This is due to the fact that the stable spin direction is tilted away from the vertical direction thereby resulting in a smaller projection of the injected polarization onto the stable spin direction.

6.2 Data Analysis for 106.9 MeV and 107.8 Incident Beam Energies

In one interesting situation, the polarization was measured at two incident beam energies, 106.9 and 107.8 MeV, during the same run. It is expected that the machine conditions did not change. We therefore attempt to study these two energies by using the exact same three parameters, ϕ, $|\epsilon|$, and $\arg\epsilon^*$.

The experimental data at 106.9 and 107.8 MeV are shown in Fig. 6 along with the type-3 snake analysis (dotted curves) and the results of the present analysis which include both the effects of the type-3 snake and the nearby imperfection depolarizing resonance (solid curves). The values of the type-3 snake and resonance parameters were first obtained by fitting Eqs. (26-28) to the 106.9 MeV data. Since this energy is closer to the resonance energy, the resonance parameters may be more accurately determined. They

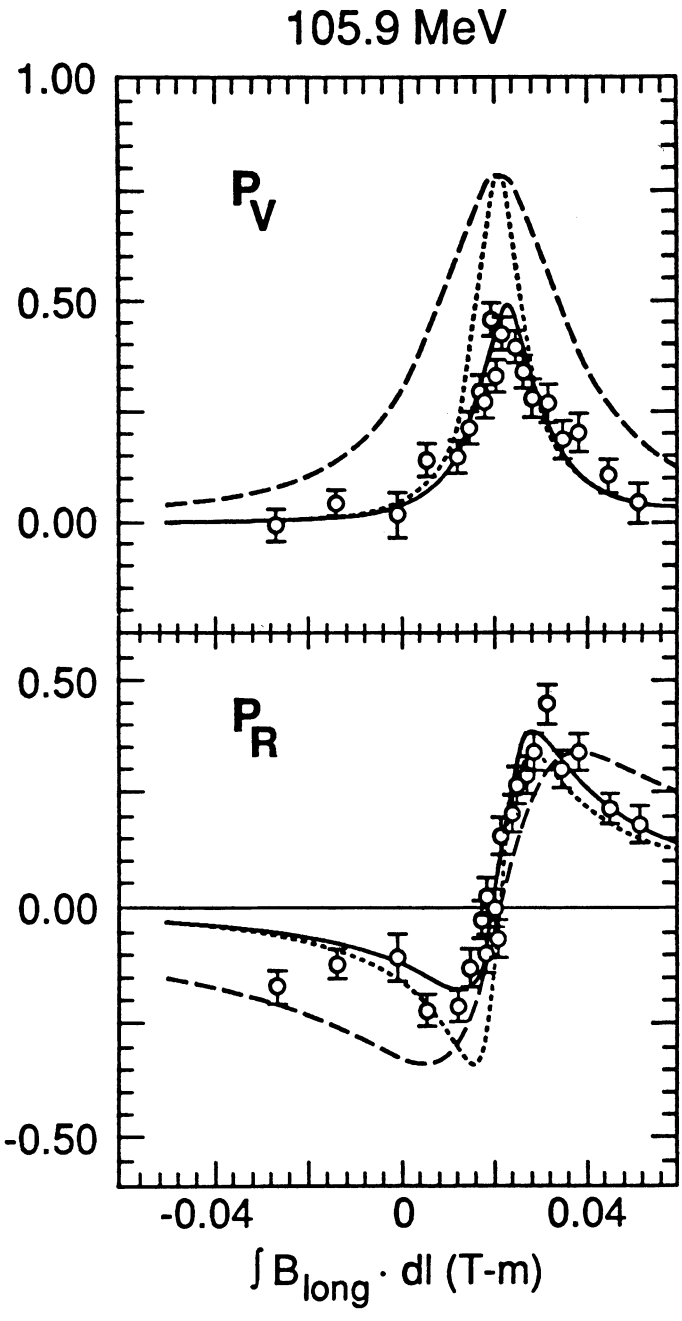

FIGURE 5: 105.9 MeV Data with Model Calculations. The 105.9 MeV vertical and radial polarization data are plotted as a function of the longitudinal field error. The curves are best fits using Eqs. (26-28). The dashed curves omit the effects of both the type-3 snake and the imperfection resonance ($\phi = 0$, $\epsilon = 0$). The dotted curves characterizes the behavior of the polarization with only a type-3 snake present in the ring ($\phi = 25$ mrad, $\epsilon = 0$). The solid curve assumes that both the type-3 snake and the $G\gamma = 2$ imperfection resonance affect the proton spin tune ($\phi = -25$ mrad, $|\epsilon| = 0.0015$, argϵ^*=4.5 mrad).

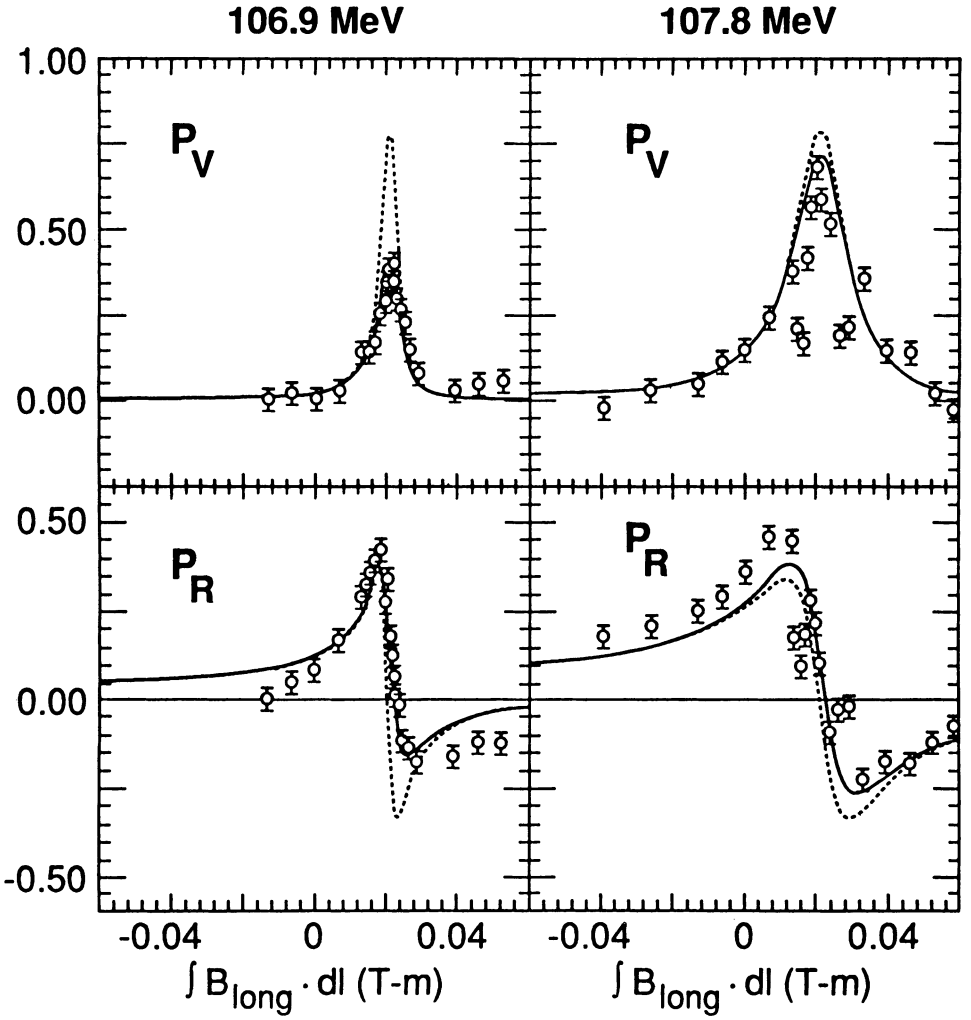

FIGURE 6: 106.9 and 107.8 MeV Data with Model Calculations. The vertical and radial polarization data are plotted as a function of the longitudinal field error. The curves for the 106.9 MeV data are best fits using Eqs. (26-28). The dotted curve shows the behavior of the polarization with only a type-3 snake present in the ring ($\phi = -34$ mrad, $\epsilon = 0$). The solid curve takes into account both the type-3 snake and the $G\gamma = 2$ imperfection resonance. The exact same set of snake and resonance parameters ($\phi = -34$ mrad, $|\epsilon| = 0.0008$, and argϵ^*=1.0 rad) are then used to predict behavior of the 107.8 MeV data.

TABLE 1: Angular Deflection of steerers in the cooling region

Incident Beam Energy [MeV]	Steerer 1 [mrad]	Steerer 2 [mrad]	Steerer 3 [mrad]	Steerer 4 [mrad]
104.6	-5.5	12.6	-16.9	7.5
105.9	-4.9	9.7	-10.1	8.7
106.9	-5.2	12.2	-17.0	7.4
107.8	-5.2	12.2	-17.1	7.3
Average	-5.2	11.7	-15.3	7.7

are $|\epsilon| = 0.0008$, $\arg\epsilon^* = 1.0$ rad, with $\phi = -34$ mrad. These same parameters were then used to predict the expected behavior of the polarization at 107.8 MeV. Taking into account both the type-3 snake and the $G\gamma = 2$ imperfection resonance (solid curves), the agreement with the experimental data is improved. Both the peak in the measured vertical polarization and the asymmetry in the measured radial polarization are reproduced using the strength parameters extracted from the 106.9 MeV data.

7 CONCLUSION AND DISCUSSION

The Thomas-BMT spin equation of motion was used to analyze experimental data[5,8] from the IUCF Cooler Ring near the $G\gamma = 2$ imperfection resonance. Analytic expressions for the spin tune and polarization components were derived in the presence of a type-3 snake[8,9], which resulted[7] from the confinement fields of the electron cooling system. Since the spin tune shift depends bilinearly on the vertical steerer and the solenoidal angles, the type 3 snake is impractical for use in jumping through imperfection resonances. Using a global fit to the data across the energy range for fixed energy and vertical injected polarization, the effective steerer spin precession angle was found to be -30 mrad. The analysis showed that the type-3 snake lowered the energy at which the imperfection depolarizing resonance occurred by about 1.9 MeV.

The effective steerer angle of -30 mrad corresponds to an orbital deflection angle of -15 mrad, which is in reasonable agreement with the measured steerer rotation angle of Table 1. In appendix B we discuss the possible variation of effective orbit angle due to the vertical closed orbit and quadrupole misalignments in the cooling region. A 0.2mm quadrupole misalignment error can cause a variation of ± 5 mrad in the effective steerer angle.

Using an effective steerer angle of -30 mrad, both the width of the vertical polarization and the slope of the radial polarization through the zero crossing were fairly fit at energies far from the resonance. The type-3 snake calculations failed, however, in the immediate vicinity of the resonance; they predicted full polarization at all energies when the longitudinal field error was fully compensated and an asymmetric radial polarization profile.

Inclusion of the $G\gamma = 2$ imperfection resonance yielded new insight into the behavior of the polarization in close proximity to the resonance. Firstly, the spin tune was shifted from $G\gamma$ by $\Delta\nu_s = -|\epsilon|$ below the resonance and by $\Delta\nu_s = |\epsilon|$ above the resonance.

Secondly, the magnitude of the vertical polarization was found to depend on the resonance strength. The resonance strength parameters and the steerer precession angle in the type-3 snake depended upon the parameters of the ring when the measurements were made. Finally, neglecting small contributions due to an injection mismatch, the imperfection resonance was seen to be responsible for the observed asymmetry in the radial polarization.

The imperfection resonance strength parameters were deduced using two data sets at 106.9 and 107.8 MeV, which were taken during the same running period. The measured radial and vertical polarization profiles at 106.9 MeV were first fit using a model with only three parameters: the effective steerer angle of the type-3 snake, the resonance strength, and the resonance phase. The same set of three parameters were then used to predict the measured polarization at 107.8 MeV. The prediction agreed fairly with the experiment on the maximum vertical polarization and the amount of asymmetry in the radial polarization. At large values of the longitudinal imperfection field, however, there were statistically significant deviations which are not yet understood.

8 ACKNOWLEDGEMENTS

We would like to thank E.D. Courant, A.D. Krisch, R.E. Pollock, and T. Roser for their many useful suggestions. We are especially indebted to A. D. Krisch for his encouragement in carrying out the theoretical analysis. We are also grateful to the research team of Cooler experiments CE05, CE15, and CE20. This research was supported by grants from the U.S. Department of Energy and the U.S. National Science Foundation.

9 APPENDIX A. Effect of a Nonvertical Injected Polarization Vector

The polarization components calculated in the type-3 snake analysis were obtained assuming a vertically polarized injected beam. In reality, the initial polarization may not be exactly vertical. The effect of an injection mismatch may result in an asymmetry in the measured polarization with respect to the longitudinal field error, $\int B_{\|} dl$.

Taking into account a mismatch at injection, let the injected polarization vector be replaced by

$$P_{inj}(\cos\beta_x, \cos\beta_s, \cos\beta_y), \tag{A1}$$

where the directional cosines satisfy the normalization, $\cos^2\beta_x + \cos^2\beta_s + \cos^2\beta_y = 1$. The resultant polarization is given by the projection of the injected polarization vector on the stable spin vector, $\vec{n}_s$; i.e.

$$\|P\| = P_{inj}(\cos\beta_x \cos\alpha_x + \cos\beta_s \cos\alpha_s + \cos\beta_y \cos\alpha_y). \tag{A2}$$

The components of the resultant polarization vector are then obtained by projecting the polarization onto the three coordinate axes:

$$P_V = \|P\| \cos\alpha_y; \quad P_R = \|P\| \cos\alpha_x; \quad P_L = \|P\| \cos\alpha_s. \tag{A3}$$

Using the same approximation as that of Eqs.(14-16) in which nominally vertically polarized beam is injected into the ring and taking into account a possible mismatch at injection, the final vertical and radial polarization components can be expressed as,

$$P_v = P_{inj}\{\cos\beta_y \cos^2\alpha_y + \frac{\sin(\psi_c - \psi)}{2\sin^2\pi\nu_s}\} \tag{6}$$
$$\times [\cos\beta_x \sin G\gamma(\pi-\theta) - \cos\beta_s \cos G\gamma(\pi-\theta)] \sin(G\gamma\pi - \frac{\psi_c\phi}{2})\},$$

$$P_R = P_{inj}\{\cos\beta_y \frac{\sin(\psi_c - \psi)}{2\sin^2\pi\nu_s} \sin G\gamma(\pi-\theta)\sin(G\gamma\pi - \frac{\psi_c\phi}{2}) \tag{7}$$
$$+\frac{\sin^2\frac{\psi_c-\psi}{2}}{\sin^2\pi\nu_s}[\cos\beta_x \sin G\gamma(\pi-\theta) - \cos\beta_s \cos G\gamma(\pi-\theta)]\sin G\gamma(\pi-\theta)\}.$$

Thus when the injection polarization is not exactly vertical ($\cos\beta_x \neq 0$; and/or $\cos\beta_s \neq 0$), the vertical polarization, P_v, will exhibit an asymmetry as a function of the effective longitudinal field error, $\psi_c - \psi$. Similarly, the radial polarization will exhibit an asymmetry.

An important feature in the asymmetry due to the mismatch at injection is that the asymmetry in the radial polarization is of second order in the longitudinal field error, i.e. it depends upon $(\psi_c - \psi)^2$. Since $\psi_c - \psi$ is small, the vertical polarization will exhibit a much more pronounced asymmetry than the radial polarization as a function of the longitudinal error field.

The behavior of the polarization is predicted assuming that the injected polarization has been precessed away from the vertical into the horizontal plane. The calculations are performed at 107.8 MeV (see Fig. 3) and use the exact form of Eqs. (A4,A5) with no small angle approximations as well as the additional effects arising from the $G\gamma = 2$ imperfection resonance. The results may be compared to Fig. 6. Plotted in the first column of Fig. 7 is the vertical and radial beam polarization assuming a large longitudinal component: $P_{inj}(\cos\beta_x, \cos\beta_s, \cos\beta_y) = (0.078, 0.331, 0.702)$. The polarization assuming a large radial component, $P_{inj}(\cos\beta_x, \cos\beta_s, \cos\beta_y) = (0.312, 0.135, 0.702)$, is plotted in the second column. As can be seen, any attempt to improve the fit by taking into account a possible mismatch at injection introduces an asymmetry in the vertical polarization, which is not reflected in the data. The data analysis indicates that the effect of an injection mismatch in the present experiments is small; the measured vertical polarization profiles are almost purely symmetric in the longitudinal field error.

10 APPENDIX B. Effective Orbit Steerer Angle in the Cooling Region due to Closed Orbit Motion

Table 1 shows the orbital deflection angles of the steerers in the cooling region. The orbital kick angles were calculated using known operating currents and magnet calibrations. Deflection angles labeled 1 and 4 are comprised of the sum of the orbital kick angles of the two outermost vertical steerers and two correction windings. Deflection

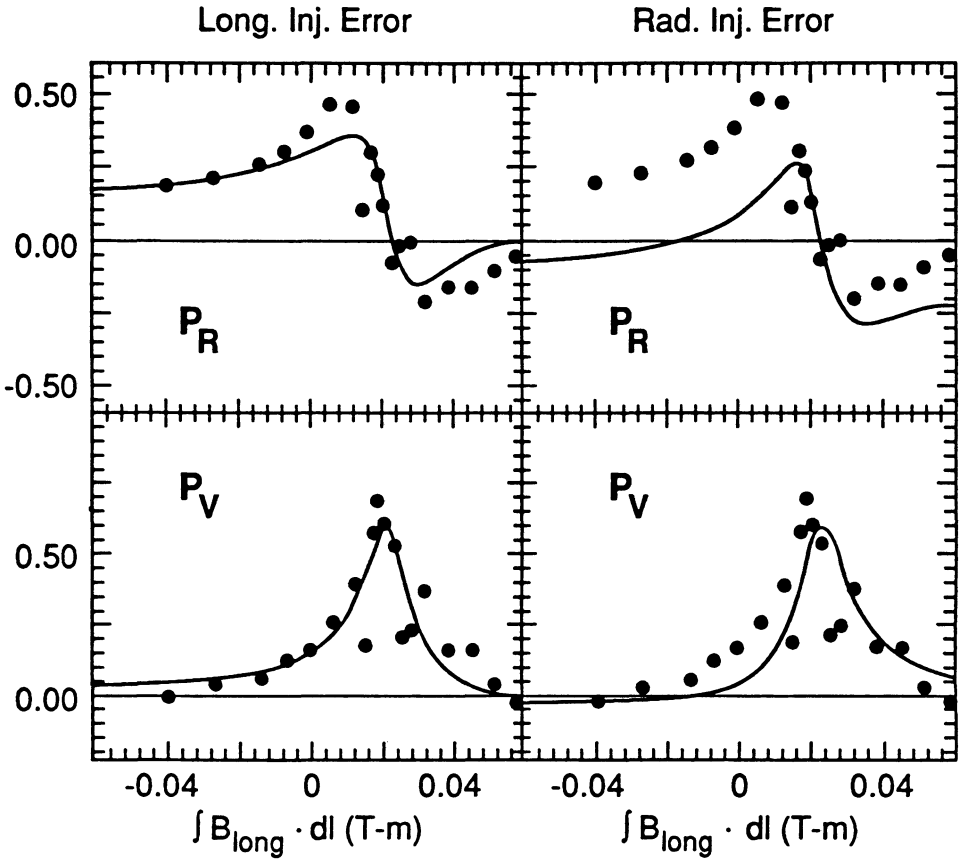

FIGURE 7: 107.8 MeV Data with Injection Error. The vertical and radial polarization data at 107.8 MeV with vertically polarized injected beam are plotted as a function of longitudinal field error. The curves are obtained from the more general form of Eqs. (A4,A5) in which no small angle approximations are made along with the additional effects arising from the $G\gamma = 2$ imperfection resonance. On the left the injected polarization is assumed to have a large longitudinal component; i.e. $||P|| = (0.078, 0.331, 0.702)$. On the right the injected polarization is assumed to have a large radial component; i.e. $||P|| = (0.312, 0.135, 0.702)$.

angles 2 and 3 take into account the sum of the inner steerers and the kick due to the radial field of the toroids (see Fig. 1).

In our analysis of the type-3 snake we assumed that the kick angles 1 through 4 were identical. Using the global fit of Eqs. (12-13) to the experimental data (see Fig. 3) the effective spin precession angle was determined to be -30 mrad. This corresponds to an orbital deflection angle of $\frac{-30}{G\gamma} = -15$ mrad near the $K = 2$ imperfection resonance. The result agrees to 10% with the average deflection angle of steerers 2 and 3.

The average of the steerers 1 and 4 is 6.5 mrad while the average of steerers 2 and 3 is 13.5 mrad. The difference is due to the fact that the beam passes through quadrupoles off-center between the steerer pairs (1,2) and the steerer pairs (3,4) respectively. In this appendix, we examine the orbital deflection angle due to quadrupole misalignments. We take into account the focussing and defocussing quadrupoles that were located between each of the compensating solenoids and the outermost vertical steerers and show that quadrupole misalignments and typical size closed orbit errors may easily lead to an enhancement in the angular deflection angles 1 and 4.

Let y_{in} be the vertical displacement and y'_{in} be the angular displacement at the entrance to the vertical steerer, VS. Using the Cooler Ring lattice and the thin lens approximation, (y_{out}, y'_{out}) at the entrance to the compensating solenoid, CS, is given by

$$\begin{pmatrix} y_{out} \\ y'_{out} \\ 1 \end{pmatrix} = \begin{pmatrix} 1 & 0 & 0 \\ \frac{1}{f_2} & 1 & \frac{\Delta y_2}{f_2} \\ 0 & 0 & 1 \end{pmatrix} \begin{pmatrix} 1 & D_2 & 0 \\ 0 & 1 & 0 \\ 0 & 0 & 1 \end{pmatrix} \begin{pmatrix} 1 & 0 & 0 \\ -\frac{1}{f_1} & 1 & -\frac{\Delta y_1}{f_1} \\ 0 & 0 & 1 \end{pmatrix} \begin{pmatrix} 1 & D_1 & 0 \\ 0 & 1 & 0 \\ 0 & 0 & 1 \end{pmatrix} \begin{pmatrix} 1 & 0 & 0 \\ 0 & 1 & \theta_k \\ 0 & 0 & 1 \end{pmatrix} \begin{pmatrix} y_{in} \\ y'_{in} \\ 1 \end{pmatrix} \quad (2)$$

where θ_k (= 6.5 mrad) is the average orbital kick angle of the vertical steerers 1 and 4, D_1 and D_2 are drift lengths equal to 0.3185 and 0.5310 m, respectively, f_1 and f_2 are the focal lengths in focussing and defocussing quadrupoles equal to 0.8591 and 0.7862 m, respectively, and Δy_1 and Δy_2 are alignment errors of the quadrupoles. Eq. (B1) gives us

$$y'_{out} - y'_{in} = (1 + \frac{D_1 + D_2}{f_2} - \frac{D_1 D_2}{f_1 f_2})\theta_k + \text{ misalignment errors.} \quad (B2)$$

Thus the quadrupoles gives an enhancement of angular kick by a factor of 1.83.

This estimation of the effects of closed orbit errors and beam displacements in the quadrupoles shows that even with no closed orbit errors at the entrance to the cooler region, an effective orbit steerer angle is -12 mrad, which is consistent with the measured angle of steerers 2 and 3. The remaining discrepancy of -3 mrad can be accounted for by the possible closed orbit errors.

REFERENCES

1. Ya.S. Derbenev and A.M. Kondratenko, *Part. Accel.*, **8**, 115, (1978).
2. A.D. Krisch *et al. Phys. Rev. Lett.* **64**, 1137, (1989).
3. J.E. Goodwin *et al. Phys. Rev. Lett.* **64**, 2779, (1990).

4. J.E. Goodwin, PhD dissertation, Indiana University, May, 1990 (unpublished).
5. M.G. Minty, PhD dissertation, Indiana University, September, 1991 (unpublished).
6. The energy calibration is based on a time of flight measurement in which a 200 keV energy spread at 300 MeV was measured.
7. R.E. Pollock, *Nucl. Instr. Meth.,* **A300**, 210, (1991).
8. M.G. Minty *et al.*, *Phys. Rev.* **D44**, 1361, (1991).
9. T. Roser, Comment at the 1990 Partial Siberian Snake Workshop at the BNL, Upton, New York (unpublished).
10. L.H. Thomas, *Philos. Mag.,* **3**, 1, (1927).
11. V. Bargman, L. Michel, V.L. Telegdi, *Phys. Rev. Lett.,* **2**, 435, (1959).
12. M. Froissart and R. Stora, *Nucl. Instr. Meth.,* **7**, 297, (1960).
13. S. Tepikian, S.Y. Lee, E.D. Courant, *Part. Accel.,* **17**, 1. (1986).
14. D. Cohen, *Rev. Sci. Instr.* **33**, 161 (1962).
15. E.D. Courant, BNL Report EDC-45 (1962) (unpublished).
16. E.D. Courant, R.D. Ruth, BNL 51270, (1980) (unpublished).
17. B.W. Montague, *Phys. Rep.* No. 113 (1984).
18. S.Y. Lee, S. Tepikian, *Phys. Rev. Lett.*, **56** 1635, (1986).
19. L. Ahrens, "Proc. of High Energy Spin Physics", *AIP Conf. Proc.*, K.J. Heller, ed., **No. 187**, 1068, (1988).
20. E.D. Courant, private communication.